Geophysical Research Letters

RESEARCH LETTER
10.1029/2023GL102951

Influences Driving and Limiting the Efficacy of Ice Segregation in Alpine Rocks

T. Mayer[1,2], M. Eppes[3], and D. Draebing[1,4]

[1]Chair of Geomorphology, University of Bayreuth, Bayreuth, Germany, [2]Chair of Landslide Research, Technical University of Munich, Munich, Germany, [3]Department of Geography & Earth Sciences, UNC Charlotte, Charlotte, NC, USA, [4]Department of Physical Geography, Utrecht University, Utrecht, the Netherlands

Key Points:

- Initial saturation levels do not limit the efficacy of ice segregation in fractured alpine rocks
- Rock initial crack density impacts rock stiffness and thermal properties and thus frost cracking efficacy
- The "frost cracking window" temperature range is dependent on rock strength and crack-controlled porosity in alpine rocks

Supporting Information:

Supporting Information may be found in the online version of this article.

Correspondence to:

T. Mayer,
till.mayer@uni-bayreuth.de

Citation:

Mayer, T., Eppes, M., & Draebing, D. (2023). Influences driving and limiting the efficacy of ice segregation in alpine rocks. *Geophysical Research Letters*, *50*, e2023GL102951. https://doi.org/10.1029/2023GL102951

Received 19 JAN 2023
Accepted 18 JUN 2023

Abstract Rockwall erosion by rockfall is largely controlled by frost weathering in high alpine environments. As alpine rock types are characterized by crack-dominated porosity and high rock strength, frost cracking observations from low strength and grain supported pore-space rocks cannot be transferred. Here, we conducted laboratory experiments on Wetterstein limestone samples with different initial crack density and saturation to test their influence on frost cracking efficacy. We exposed rocks to real-rockwall freezing conditions and monitored acoustic emissions as a proxy for cracking. To differentiate triggers of observed cracking, we modeled ice pressure and thermal stresses. Our results show initial full saturation is not a singular prerequisite for frost cracking. We also observe higher cracking rates in less-fractured rock. Finally, we find that the temperature threshold for frost cracking in alpine rocks falls below −7°C. Thus, colder, north-exposed rock faces in the Alps likely experience more frost cracking than southern-facing counterparts.

Plain Language Summary Freezing results in the formation of ice that exerts stresses on fracture walls and draws in additional moisture to supply further growth and break down rocks, a process termed frost cracking. Frost cracking drives much erosion and rockfall in alpine environments. Here we test hypotheses from prior work about how frost cracking is impacted by saturation and rock properties. We exposed rock samples of different strength and saturation to identical freezing conditions in laboratory experiments. We monitored rock temperature and acoustic emissions (AE), assuming frost cracking produces the recorded AE hits. We find that initial full saturation is not required for frost cracking, as water transport is enhanced by fractures in alpine rocks. Furthermore, rock with initial higher short-term strength showed more frost cracking because, we infer, of stiffness properties that make these rocks more brittle compared to lower strength rocks. Frost cracking occurred at a wide range of temperatures below freezing and was highest between −9 and −7°C. We thus conclude that frost cracking is most impacted by temperature and rock short-term strength. In Alpine environments, this may result in more frost cracking and rockfall on colder north-facing rockwalls than warmer southern exposures.

1. Introduction

In the European Alps, present-day rockwall erosion by rockfall processes shape rockwalls with rates between $0.05^{+0.03}_{-0.03}$ mm a^{-1} to 14.4 mm a^{-1} (Draebing et al., 2022). These rates are in the same order of magnitude as glacial erosion rates (0.5–36 mm a^{-1}; Cook et al., 2020) suggesting that rockfall processes are key agents of alpine landscape evolution. Rockwall erosion is controlled by permafrost (Krautblatter et al., 2013), glacier retreat (Hartmeyer et al., 2020), frost cracking (Hales & Roering, 2005) or a combination of these processes (Draebing et al., 2022). Ice segregation is a dominant frost weathering process capable of breaking rocks (Matsuoka & Murton, 2008). Previous studies suggest that certain rock temperature ranges "frost cracking window" and rock moisture levels (Sass, 2005a), rock strength and fracture density (Walder & Hallet, 1985) can control the efficacy of frost cracking, however, to date no study has experimentally quantified specifically how these controlling factors directly impact frost cracking processes, a key connection for fully understanding alpine rockfalls and associated landscape evolution.

Previous experimental studies investigating the temperature ranges controlling frost cracking employed high-intergranular-porosity sedimentary rocks with relatively low rock short-term strength (hereafter strength). For example, Hallet et al. (1991) observed highest frost cracking activity in Berea Sandstone (~20% mostly intergranular porosity) between −6 and −3°C while Murton et al. (2006) observed ice segregation in weak chalk

starting below the pore freezing point. In contrast, alpine rocks are characterized by fracture- or crack-dominated pore space and high overall rock strength that may influence the temperature range at which frost cracking is effective. Theoretical models suggest that frost cracking depends on fracture toughness (Rempel et al., 2016; Walder & Hallet, 1985) and occurs between −15 and −4°C (Walder & Hallet, 1985). Thus, specific frost cracking temperature ranges depend on site-specific conditions. For example, field measurements of acoustic emission (AE) signals on gneiss rockwalls showed frost cracking within a temperature range of −15 to −1°C (Girard et al., 2013), but in other work derived from recorded rock temperature profiles, Anderson (1998) found a "frost cracking window" for granite between −8 and −3°C. Overall, the application of a fixed "window" across different rock types and field sites is not advisable because it can produce non-reliable results (Draebing & Mayer, 2021) by oversimplifying temperature control.

Similarly, a minimum effective saturation has been found for volumetric ice expansion in laboratory studies (Jia et al., 2015; Prick, 1997), however, a similar lower threshold for ice segregation-induced frost cracking has yet to be identified. Ice stresses are caused by water flux along water films surrounding ice crystals resulting in ice crystal growth (e.g., Gerber et al., 2022; Sibley et al., 2021). Rockwall saturation in high alpine environments varies with aspect and rock mass depth (Girard et al., 2013; Sass, 2005a). Laboratory studies by Draebing and Krautblatter (2019) suggested that ice segregation can occur at low initial saturation levels as long as water is available to migrate—a condition provided by alpine rock masses (Sass, 2005a).

In sum, rockwalls are characterized by fractures that increase water transport (Dietrich et al., 2005), weathering activity (Shmilovitz et al., 2022) and erodibility (Neely et al., 2019) suggesting that weathering processes including frost cracking may be influenced by initial fracture and water content. In this study, we perform ice segregation tests on rock samples with different saturation levels and fracture density to quantify their influence on frost cracking efficacy.

2. Experimental Setup

The setup was inspired by Hallet et al. (1991) whose experiments isolated ice segregation from other weathering processes. We performed freezing tests on three $0.2 \times 0.2 \times 0.4$ m large Wetterstein limestone samples (Figure 1a and Figure S1 in Supporting Information S1), representing the abundant lithology of Northern Calcareous Alps. Throughout, we use the term "fracture" to describe any low-aspect-ratio discontinuity and "cracking" to refer to the process of fracture propagation. Samples were excavated from a quarry with varying fracture density. Therefore, we sampled both highly fractured (high-porosity) and minimally fractured (low-porosity) specimens (Text S1 in Supporting Information S1). Rock properties were quantified using laboratory measurements (Lepique, 2008; Zhang, 2002). Rock sample 1 (R1) contained no visible fractures and an initial rock porosity of 0.4%. Rock samples 2 (R2) and 3 (R3) were characterized by visible initial fractures and a higher initial porosity of 0.6% (Figure 1a).

We applied a submillimeter film of epoxy resin to the sides, but not bottom and top, of the blocks to prevent lateral water infiltration. We fully saturated the low-porosity R1 and the high-porosity R2 but kept the high-porosity R3 room-dry to maintain a natural low moisture content between 5% and 10% (volumetric water content). For each experiment, all rock samples were surrounded with a minimum of 4 cm Styrofoam insulation leaving the bottoms and tops open.

The rock samples were put in a cooling chamber (Kambič KK-340 CHLT) with the top exposed to freezing conditions, while the bottom of the samples was placed in a water bath that was kept above the freezing point using a Freek heater (Figure 1b). This setup simulates an open system and enables the development of a linear temperature gradient inside the rock body with a water reservoir providing moisture. We monitored rock temperature at a lateral distance of 10 cm into the interior of each sample at 4, 15, 25, and 36 cm depth from the top using four Greisinger Pt 1000 temperature sensors (0.03°C accuracy). To test realistic frost cracking efficacy, rock samples were all exposed to identical temperature cycles reflecting rock temperatures in the Northern Calcareous Alps (Figure 1c and Table S2 in Supporting Information S1). Rocks were cooled from ∼10°C rock temperature at the upper surface to −9.5°C within one day (Figure 1d). Afterward, air temperature was raised by 2°C every 50 hr and kept at a steady state for 40 hr enabling ice segregation and excluding the occurrence of other weathering processes (Hallet et al., 1991) (Text S2 in Supporting Information S1).

To monitor cracking, we installed two Physical Acoustics AE sensors PK6I (frequency 35–65 kHz) at the top and at the side of each block. AE data was recorded using a Physical Acoustics Micro SHM node as well as

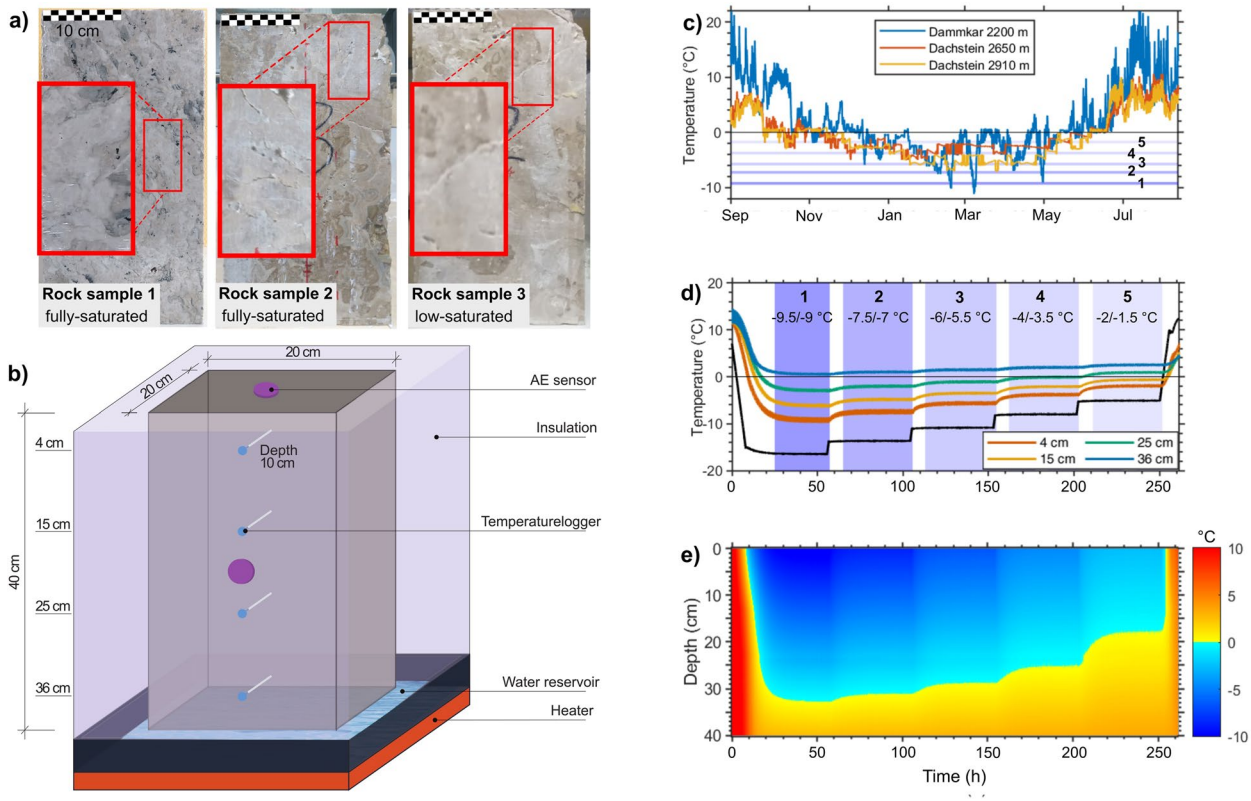

Figure 1. Photos of (a) rock samples and (b) schematic visualization of laboratory setup. (c) Exemplary rockwall temperatures for sites in the Northern Calcareous Alps. (d) Measured rock temperatures at different depth, air temperature (black) and (e) modeled rock temperatures at sample R3 plotted against time.

analyzed and filtered using Physical Acoustics AEwin software (Text S3 in Supporting Information S1). AE signals were differentiated into signals ≤41 dB_{AE} with a broad waveform and signals >41 dB_{AE} with single crack-like waveforms (Figure S2 in Supporting Information S1). AE signals can be triggered by thermal stresses (Eppes et al., 2016) during temperature changes or by ice stresses (Hallet et al., 1991).

To interpret the drivers of AE, we modeled temperature regime inside the rocks (Text S4 in Supporting Information S1) and used recorded rock temperature to drive thermos-mechanical frost cracking (Walder & Hallet, 1985) and one-dimensional thermal stress models (Paul, 1991; Pei et al., 2016) performed using MATLAB R2021b (Text S5 and S6 and Table S3 in Supporting Information S1). Using a frost cracking model with rock property data, we employed a simplified approach to calculate the threshold stress magnitude (4 MPa) needed to propagate a 1 cm size preexisting fracture, acknowledging that fractures both larger and smaller likely exist in the samples. We use this threshold not to suggest quantifying an absolute magnitude of cracking in the block, but to define model predictions of the timing of cracking compared to measured cracking in the experiment.

3. Results

Based on rock temperature loggers at 4 cm depth, we differentiate five phases of steady state temperatures. During the initial cooling Phase-0 (10°C to −8°C; Figure 1d), AE activity (Figure 2) and modeled thermal stress magnitude (Figure 3a) and ice pressure built up (Figure 3b). We detected more than 396 hits (10% of all AE signals) for R1 (Figure 2a), 244 hits (20%) for R2 (Figure 2b) and 763 (30%) for R3 (Figure 2c) with the majority of signals (68%–82%) recorded after the rocks reached freezing temperatures. For all samples, the top sensor received over 96% of overall hits.

While rock temperatures decreased to −9°C, modeled thermal stress reached its maximum in all samples, with a pattern of decreasing magnitudes with increasing rock depth (Figure 3a and Figure S3 in Supporting Information S1). When rock temperatures reached the pore freezing point after 9 hr of cooling, modeled ice pressure in 4 and 15 cm depth showed an increase and exceeded the 4.0 MPa cracking threshold at the end of Phase-0 (Figure 3b and Figure S3 in Supporting Information S1).

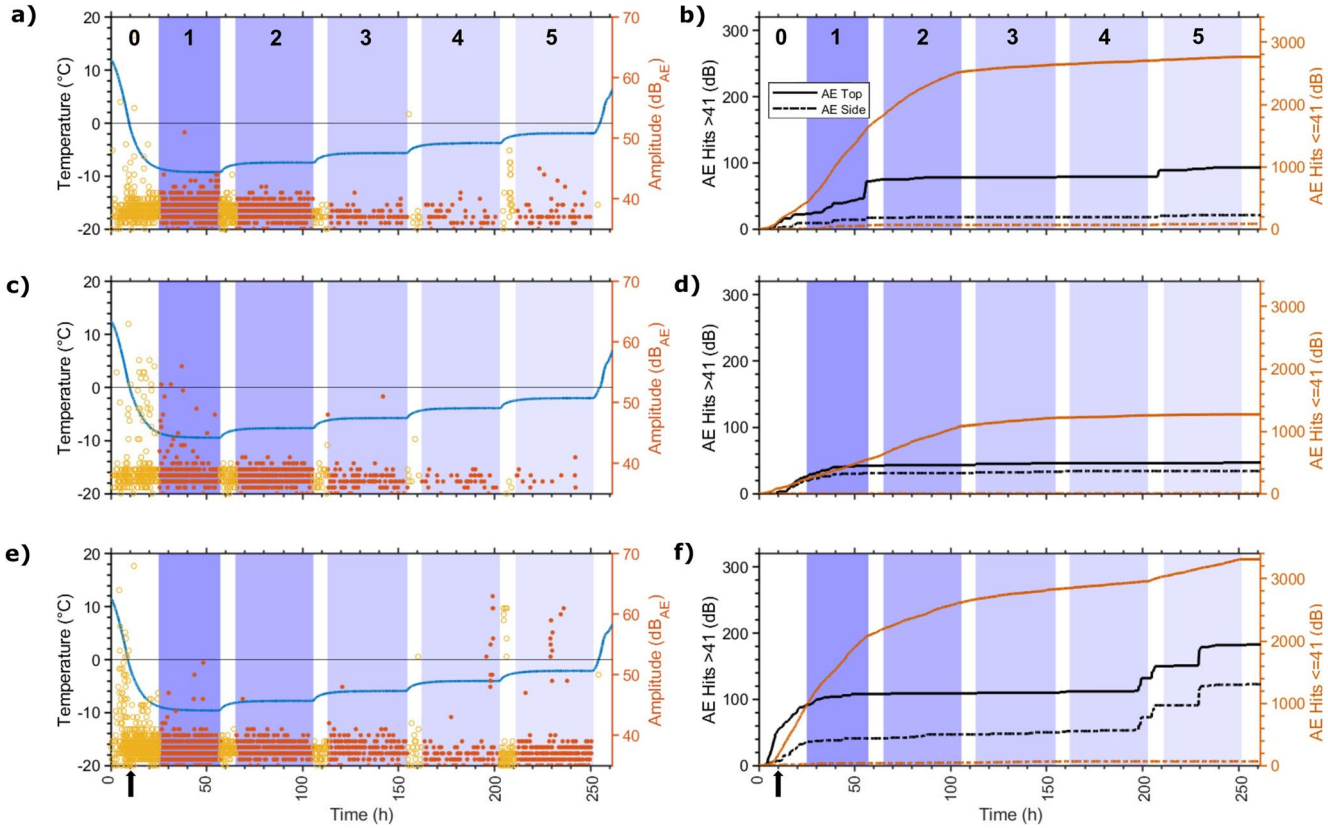

Figure 2. Acoustic emission (AE) hits differentiated into hits during changing (yellow) and steady-state temperatures (red dots) and rock temperature in 4 cm depth (blue line) plotted against time for (a) R1, (c) R2, and (e) R3. Cumulative AE hits differentiated into hits ≤41 dB_{AE} (black line) and >41 dB_{AE} (orange line) plotted against time for (b) R1, (d) R2, and (f) R3. The arrow highlights when temperatures at 4 cm depth undergo 0°C.

During the steady temperature phases, the top logger recorded over 98% of all AE hits with amplitude equal or below 41 dB_{AE}. Phase-1 was characterized by a steady rock temperature regime between −9.5 and −9°C (Figure 1d), with the most AE hits detected, highest fracture growth in frost cracking modeling and a minimum thermal stress. All rock samples showed the strongest increase in overall AE hits with 965 hits (45%) for R1 and 313 and 862 hits (30%) for R2 and R3 (Figure 2). During Phase-1 but also Phases 2–5, thermal stress decreased to zero for all samples (Figure 3a). Modeled frost cracking showed an increase in ice pressure during Phase-1, which reached its maximum 7.5 MPa at 4 cm and 6.0 MPa at 15 cm depth (Figure 3b and Figure S3 in Supporting Information S1). Modeled fracture length increases significantly at both depths as ice pressure already exceeded its critical threshold.

Between phases, air and rock temperatures were increased by 1–2°C (Figure 1d), resulting in local maxima of thermal stress and low AE activity. Between Phase-1 and -2, AE hits were recorded at all samples (Figure 2), however, only one hit exceeding 41 dB_{AE} occurred at R3. Between Phase-2 and -3 as well as –3 and –4 this pattern repeated for the other samples with only one to two hits above 41 dB_{AE}. In contrast, higher number of AE were measured between Phases-4 and -5 with seven at R1 and R3.

Phase-2, characterized by rock temperatures at −7.5 to −7°C, revealed the second highest AE activity (Figure 2) and second highest modeled fracture growth (Figure 3b). Between one and five AE hits above 41 dB_{AE} were detected. In contrast, signals with lower amplitude ranged from 387 (12%) for the R3 to 418 hits (34%) for R2 and 601 hits (21%) for R1. Frost cracking models showed a decrease in ice pressure at 4 and 15 cm depths as temperature started to warm which resulted in a flattening of the predicted fracture growth curve (Figure 3b and Figures S3b and S3d in Supporting Information S1).

Phase-3 (−6 to −5.5°C) showed a decrease in AE activity and modeled ice pressure. Sensors recorded a low number of AE hits with only two and four hits at R2 and R3 above 41 dB_{AE}. Below 41 dB_{AE}, 91 hits (R1 3%), 110 hits (R2 9%) and 169 hits (R3 5%) were recorded. Frost cracking modeling revealed decreasing ice pressure with ice pressure at 4 cm depth exceeding the critical threshold but barely increasing fracture length.

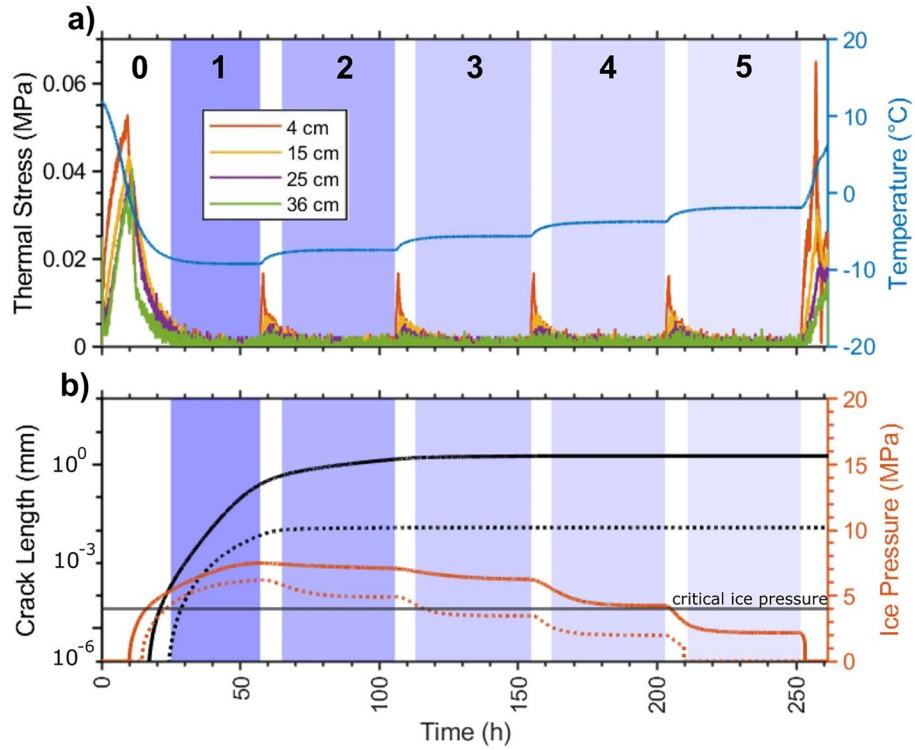

Figure 3. (a) Measured rock temperature in 4 cm depth and modeled thermal stresses for R1. (b) Modeled frost cracking (black) and ice pressure (orange line) for rock depth at 4 cm (solid) and 15 cm depth (dotted line) for R1.

In Phase-4 (−4 to −3.5°C), measured AE activity and modeled ice pressure further decreased. AE signals with amplitude above 41 dB_{AE} were detected for R1 and R2, but at the end of the phase R3 showed a cluster of 12 hits (4%). Signals with lower amplitude were also reduced to 49 (2%) for R1, 35 hits (3%) for R2 and 106 hits (3%) for R3. Frost cracking modeling showed that ice pressures at 4 cm depth dropped below the critical threshold and fracture growth ceased.

In Phase-5 (−2 to −1.5°C), AE activity slightly increased, which is not predicted by the frost model. AE signals increased for R1 with four hits (3%), R2 with one hit (1%) and R3 with 14 hits (5%) for amplitudes above 41 dB_{AE}. R1 showed 51 hits (2%) with lower amplitude, R2 13 hits (1%) and in R3 252 hits (8%) were detected. The frost cracking model showed ice pressures below the critical threshold of 4.0 MPa. In the following thawing and warming phase, only two hits with different amplitudes were detected at R1 and R3.

4. Discussion

4.1. Potential Sources Triggering AE Signals

AE signals observed during initial cooling Phase-0 are attributable to stresses arising from thermal cycling, volumetric expansion, and ice segregation, each of which could result in fracture propagation by itself or in combination (Eppes & Keanini, 2017). A large overall portion (>20%) of AE hits occurred during Phase-0, with most after the rock reached freezing temperatures. Rapid decreasing temperatures resulted in high modeled thermal stress (Figure 3a). Although our applied thermal stress model potentially overestimates thermal stress magnitudes by neglecting fracture geometries, the model enables us to analyze thermal stress timing. Field studies by Eppes et al. (2016) and Loope et al. (2020) demonstrated that rapid changing temperatures lead to AE-producing fracture propagation by thermal stresses.

We cannot rule out that post-freezing increases in AE (Figures 2a–2d) in samples R1 and R2 were triggered by volumetric expansion of in situ freezing water, because their moisture levels exceed the experimentally derived required saturation threshold of 58% (Prick, 1997) or >91% (Walder & Hallet, 1986). However, R3 revealed even a higher number of AE events (Figures 2e and 2f) despite low initial saturation (5%–10%), bringing into question the role of volumetric expansion. Our modeling predicted ice pressure development at the end of Phase-0 that

could trigger AE events (Figure 3b). However, given the simplification of fracture geometries in the model, the timing of the stresses should be given more weight than their modeled magnitude. Potential error sources for AE signals are discussed in Text S3 of Supporting Information S1.

Our results suggest that AE signals during steady temperature phases are triggered by ice segregation because our steady-temperature experimental set-up precludes stresses arising from thermal cycling, volumetric expansion, and ice deformation (Hallet et al., 1991). Also, during Phases 1–5, the top logger recorded over 98% of all AE hits with amplitude equal or below 41 dB_{AE} suggesting that AE hits were mostly generated at the top part of the sample, where frost cracking models revealed highest ice pressures.

In Phase-5, we observed a small increase of AE hits (Figure 2). Rising temperatures could increase water availability and water movement either by gravity or by ice segregation (Walder & Hallet, 1985). Such liquid water can increase cracking rates, even under steady or lowering stress magnitudes, and refreezing of water could also trigger AE signals.

4.2. Initial Rock Moisture Is Not a Primary Control of Ice Segregation

Our data suggest that the efficacy of ice segregation is not limited by initial water content in alpine rocks. R2 and R3 possess similar fracture density but initial water saturation varied between low saturation (R3) and fully saturated (R2). However, both samples revealed the same pattern of increased AE magnitudes during Phase-1 and -2 (Figures 2c–2f), characterized by AE hits with amplitudes ≤41 dB_{AE} while hits with amplitudes >41 dB_{AE} were limited to Phase-1. The low-saturated R3 exhibited a higher accumulation of AE than higher-saturated R2. This pattern could result from freezing of in-situ water in R2 that increases rock strength (Han et al., 2022). More ice lenses form compared to low-saturated rock. The lenses possibly compete with each other and also increase rock strength. As our frost cracking model uses singular lenses, we cannot predict the effect of neighboring ice lenses.

The observed AE pattern may indicate either that capillary rise from the water bath promoted ice segregation or that the initial low saturation was sufficient for ice segregation. By using a similar set-up, Draebing and Krautblatter (2019) observed that water migration enabled ice segregation in open fractures for initially unsaturated alpine rock samples. Furthermore, measured and modeled water content in limestone rockwalls revealed moisture levels of 70% and higher below 10 cm depths (Rode et al., 2016; Sass, 2005a). Thus, the use of a water bath in laboratory studies (Hallet et al., 1991; Murton et al., 2006) seems a reasonable approach to simulate natural rockwall moisture regimes. In rockwalls, rock water transport is controlled by fractures (Dietrich et al., 2005), which can rapidly transport water within the rock mass (Phillips et al., 2016). On south-exposed rockwalls under relatively dry conditions, Girard et al. (2013) recorded AE events and interpreted these as frost cracking-induced. Therefore, our data suggest that ice segregation could potentially occur in initially dry rocks (5%–10% saturation) by either water migration as capillary rise or by cryosuction.

4.3. Fracture Density Controls Frost Cracking

Our results suggest that fracture density controls susceptibility to thermal stress and frost cracking, with higher fracture density causing lower susceptibility. This is because stiffer rocks with fewer fractures are expected to fracture more quickly as growth rate is proportional to elastic modulus (Vlahou & Worster, 2015). Our results showed that the low-porosity R1 sample experienced over twice as many hits with amplitude ≤41 dB_{AE} and one-fourth more with higher amplitudes >41 dB_{AE} as the high-porosity sample R2 (Figures 2a–2d). This behavior is consistent with the fact that R2 exhibits higher compliance, as reflected by its lower shear- and Young's-modulus compared to R1 (Table S1 in Supporting Information S1). In addition, our thermal stress modeling predicted higher stresses at R1 compared to R2—in large part because of Young-modulus on the calculation (Figure 3a and Figure S3a in Supporting Information S1). Finally, P-wave velocity and Young-modulus increase due to freezing (Draebing & Krautblatter, 2012; Han et al., 2022), which amplifies fracture propagation (Han et al., 2022).

4.4. Rock Temperature Controls Ice Segregation Efficacy

Our data suggests that temperature significantly impacts ice segregation efficacy, and it supports the idea that the "frost-cracking window" differs between various rock types, controlled by pore-space geometry and rock strength. According to theoretical models (Walder & Hallet, 1985) and field measurements (Girard et al., 2013), ice segregation can occur at wide temperature ranges. In our experiment, we chose to rapidly decrease rock temperature followed by slow warming, reflecting commonly experienced conditions for north-facing snow-affected rockwalls

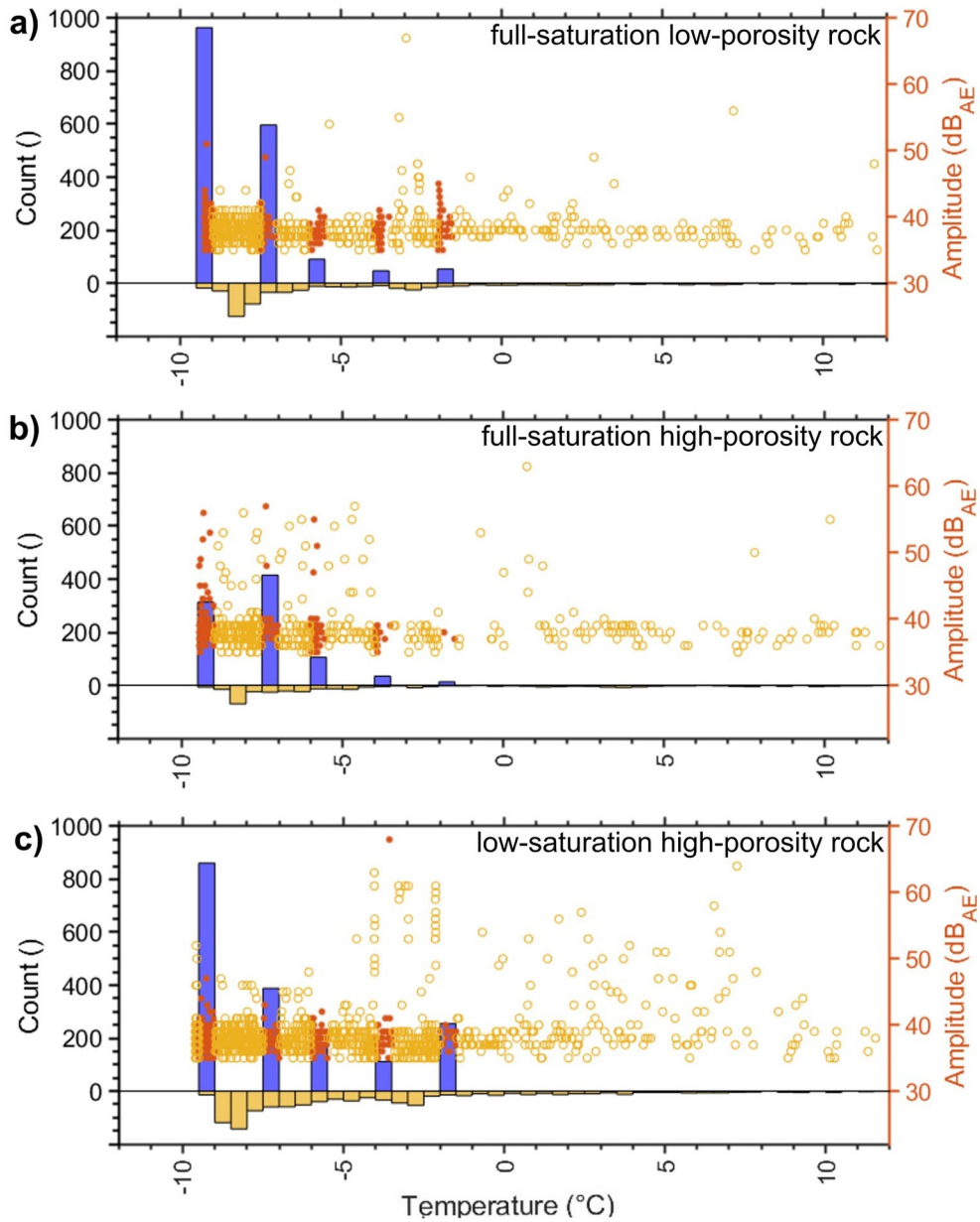

Figure 4. Number and amplitude of acoustic emission hits plotted versus rock temperature (4 cm) for (a) R1, (b) R2, and (c) R3.

in the Alps (see Dachstein in Figure 1c). We observed maximum AE between −9 and −7°C and a decrease of AE hits above −6°C (Figure 4), which differs to the studies by Hallet et al. (1991) that recorded a maximum between −6 and −3°C at Berea Sandstone and by Murton et al. (2006), where ice segregation in Tuffeau Limestone initiated just below the freezing point.

We infer from our results that low intergranular porosity and high rock strength will serve to lower the temperatures at which ice segregation is most efficacious. Fracture propagation in rock with homogeneous pore-space geometry (Berea Sandstone) will differ from that of rock with fracture-controlled porosity (Wetterstein limestone). In addition, fracture propagation is limited by rock strength (Atkinson & Meredith, 1987; Bewick et al., 2019; Segall, 1984). Fracture toughness of Wetterstein limestone (1.1 MPa $m^{1/2}$) is approximately one order of magnitude higher than fracture toughness of Berea sandstone (0.28 MPa $m^{1/2}$; Hallet et al., 1991) and Tuffeau limestone (0.2 MPa $m^{1/2}$; Murton et al., 2006). Thus, Wetterstein requires the higher stress magnitudes of lower temperatures to fracture.

In alpine rockwalls, temperature and moisture regimes differ strongly between north- and south-facing exposures (Hasler et al., 2011; Magnin et al., 2015). North-facing rockwalls are characterized by sustained low temperatures affected by snow cover (Draebing et al., 2017; Haberkorn et al., 2015) and therefore higher saturation within the upper 0.1 m of the rock surface (Rode et al., 2016; Sass, 2005a). Depending on rock temperatures before snow cover onset, the insulating snow can promote or inhibit ice segregation (Draebing & Mayer, 2021). In our experiment, we selected rapid freezing followed by slowly increasing rock temperatures representative for north-facing rockwalls with freezing before snow onset (see Dachstein in Figure 1c). Our data demonstrated a decrease of frost cracking activity with increasing temperatures (Figure 4). Other temperature scenarios like slow freezing followed by warming (see Dachstein in Figure 1c) or rapid freezing and rapid warming (see Dammkar in Figure 1c) will not affect the observed temperature range pattern in Figure 4 as even after the experiment enough fractures remain and the controlling factors as fracture toughness will remain the same.

South-facing rockwall temperatures in the Alps are warmer on average than north-facing (Hasler et al., 2011; Magnin et al., 2015) with fewer snow cover days (Draebing et al., 2017; Haberkorn et al., 2015) and reduced rock moisture in the upper 0.1 m of rock (Rode et al., 2016; Sass, 2005a). If ice segregation is not limited by initial saturation as long as water migration is possible, then there should be less frost cracking on south faces overall, which can explain observed lower erosion by rockfall compared to north-facing rockwalls (Coutard & Francou, 1989; Sass, 2005b). As south-facing rockwalls experience more frequent and higher magnitude thermal changes (Draebing & Mayer, 2021), thermal stress-related cracking in those locations may serve to offset lower frost-cracking to prepare and trigger rockfall (Collins & Stock, 2016).

5. Conclusions

Our laboratory tests reveal the role of rock mechanical and moisture properties on the temperature-dependent efficacy of ice segregation driven frost cracking in rock. The occurrence of ice segregation in our low-moisture sample (5%–10%) suggests that there is no lower moisture limit for frost cracking in alpine rocks if liquid water is available within distances in the order of 0.4 m or less. Our experiments demonstrate that water travels rapidly along fractures to form ice lenses near the outer, cold rock surface. Initial rock fracture density affects rock stiffness which determines both thermal stress and subsequent fracture propagation. Highly fractured rocks may be less prone to ice segregation because their higher compliance increases the accommodation of stresses without the need for further brittle fracture. Our data support the idea that "frost cracking window" temperatures are rock short-term strength dependent, with lower temperatures required to fracture stronger rocks. These combined results suggest that higher frost cracking efficacy associated with colder rock temperatures may result in more rockfall for north-rather than south-facing rockwalls.

Data Availability Statement

AE and temperature data can be accessed at https://doi.org/10.6084/m9.figshare.23584686.

Acknowledgments
This work was supported by the German Research Foundation (DFG) (DR1070/3-1). The authors thank Andrew Mitchell, Timo Sprenger, Manuel Löhr, and Oliver Sass for field and laboratory support. We thank the anonymous reviewer for his/her helpful comments. Open Access funding enabled and organized by Projekt DEAL.

References

Anderson, R. S. (1998). Near-surface thermal profiles in alpine bedrock: Implications for the frost weathering of rock. *Arctic and Alpine Research*, *30*(4), 362–372. https://doi.org/10.2307/1552008

Atkinson, B. K., & Meredith, P. G. (1987). The theory of subcritical crack growth with applications to minerals and rocks. In B. S. Atkinson (Ed.), *Fracture mechanics of rock* (pp. 111–166). Academic Press.

Bewick, R. P., Kaiser, P. K., & Amann, F. (2019). Strength of massive to moderately jointed hard rock masses. *Journal of Rock Mechanics and Geotechnical Engineering*, *11*(3), 562–575. https://doi.org/10.1016/j.jrmge.2018.10.003

Collins, B. D., & Stock, G. M. (2016). Rockfall triggering by cyclic thermal stressing of exfoliation fractures. *Nature Geoscience*, *9*(5), 395–400. https://doi.org/10.1038/ngeo2686

Cook, S. J., Swift, D. A., Kirkbride, M. P., Knight, P. G., & Waller, R. I. (2020). The empirical basis for modelling glacial erosion rates. *Nature Communications*, *11*(1), 759. https://doi.org/10.1038/s41467-020-14583-8

Coutard, J.-P., & Francou, B. (1989). Rock temperature measurements in two alpine environments: Implications for frost shattering. *Arctic and Alpine Research*, *21*(4), 399–416. https://doi.org/10.2307/1551649

Dietrich, P., Helmig, R., Sauter, M., Hötzl, H., Köngeter, J., & Teutsch, G. (2005). *Flow and transport in fractured porous media*. Springer.

Draebing, D., Haberkorn, A., Krautblatter, M., Kenner, R., & Phillips, M. (2017). Thermal and mechanical responses resulting from spatial and temporal snow cover variability in permafrost rock slopes, Steintaelli, Swiss Alps. *Permafrost and Periglacial Processes*, *28*(1), 140–157. https://doi.org/10.1002/ppp.1921

Draebing, D., & Krautblatter, M. (2012). P-wave velocity changes in freezing hard low-porosity rocks: A laboratory-based time-average model. *The Cryosphere*, *6*(5), 1163–1174. https://doi.org/10.5194/tc-6-1163-2012

Draebing, D., & Krautblatter, M. (2019). The efficacy of frost weathering processes in alpine rockwalls. *Geophysical Research Letters*, *46*(12), 6516–6524. https://doi.org/10.1029/2019gl081981

Draebing, D., & Mayer, T. (2021). Topographic and geologic controls on frost cracking in alpine rockwalls. *Journal of Geophysical Research: Earth Surface*, *126*(6), e2021JF006163. https://doi.org/10.1029/2021JF006163

Draebing, D., Mayer, T., Jacobs, B., & McColl, S. T. (2022). Alpine rockwall erosion patterns follow elevation-dependent climate trajectories. *Communications Earth & Environment*, *3*(1), 21. https://doi.org/10.1038/s43247-022-00348-2

Eppes, M.-C., & Keanini, R. (2017). Mechanical weathering and rock erosion by climate-dependent subcritical cracking. *Reviews of Geophysics*, *55*(2), 470–508. https://doi.org/10.1002/2017RG000557

Eppes, M. C., Magi, B., Hallet, B., Delmelle, E., Mackenzie-Helnwein, P., Warren, K., & Swami, S. (2016). Deciphering the role of solar-induced thermal stresses in rock weathering. *Geological Society of America Bulletin*, *128*(9–10), 1315–1338. https://doi.org/10.1130/b31422.1

Gerber, D., Wilen, L. A., Poydenot, F., Dufresne, E. R., & Style, R. W. (2022). Stress accumulation by confined ice in a temperature gradient. *Proceedings of the National Academy of Sciences of the USA*, *119*(31), e2200748119. https://doi.org/10.1073/pnas.2200748119

Girard, L., Gruber, S., Weber, S., & Beutel, J. (2013). Environmental controls of frost cracking revealed through in situ acoustic emission measurements in steep bedrock. *Geophysical Research Letters*, *40*(9), 1748–1753. https://doi.org/10.1002/grl.50384

Haberkorn, A., Hoelzle, M., Phillips, M., & Kenner, R. (2015). Snow as a driving factor of rock surface temperatures in steep rough rock walls. *Cold Regions Science and Technology*, *118*, 64–75. https://doi.org/10.1016/j.coldregions.2015.06.013

Hales, T. C., & Roering, J. J. (2005). Climate-controlled variations in scree production, Southern Alps, New Zealand. *Geology*, *33*(9), 701–704. https://doi.org/10.1130/g21528.1

Hallet, B., Walder, J. S., & Stubbs, C. W. (1991). Weathering by segregation ice growth in microcracks at sustained subzero temperatures: Verification from an experimental study using acoustic emissions. *Permafrost and Periglacial Processes*, *2*(4), 283–300. https://doi.org/10.1002/ppp.3430020404

Han, Y., Jia, H., Wang, T., Wang, L., Li, Q., & Wang, Y. (2022). Fracture toughness and cracking behavior of frozen sandstone at different freezing temperatures. *Engineering Fracture Mechanics*, *271*, 108664. https://doi.org/10.1016/j.engfracmech.2022.108664

Hartmeyer, I., Delleske, R., Keuschnig, M., Krautblatter, M., Lang, A., Schrott, L., & Otto, J. C. (2020). Current glacier recession causes significant rockfall increase: The immediate paraglacial response of deglaciating cirque walls. *Earth Surface Dynamics*, *8*(3), 729–751. https://doi.org/10.5194/esurf-8-729-2020

Hasler, A., Gruber, S., & Haeberli, W. (2011). Temperature variability and offset in steep alpine rock and ice faces. *The Cryosphere*, *5*(4), 977–988. https://doi.org/10.5194/tc-5-977-2011

Jia, H., Xiang, W., & Krautblatter, M. (2015). Quantifying rock fatigue and decreasing compressive and tensile strength after repeated freeze-thaw cycles. *Permafrost and Periglacial Processes*, *26*(4), 368–377. https://doi.org/10.1002/ppp.1857

Krautblatter, M., Funk, D., & Günzel, F. K. (2013). Why permafrost rocks become unstable: A rock–ice-mechanical model in time and space. *Earth Surface Processes and Landforms*, *38*(8), 876–887. https://doi.org/10.1002/esp.3374

Lepique, M. (2008). Empfehlung Nr. 10 des Arbeitskreises 3.3 "Versuchstechnik Fels" der Deutschen Gesellschaft für Geotechnik e. V.: Indirekter Zugversuch an Gesteinsproben – Spaltzugversuch. *Bautechnik*, *85*(9), 623–627. https://doi.org/10.1002/bate.200810048

Loope, D. B., Loope, G. R., Burberry, C. M., Rowe, C. M., & Bryant, G. C. (2020). Surficial fractures in the Navajo sandstone, south-western USA: The roles of thermal cycles, rainstorms, granular disintegration, and iterative cracking. *Earth Surface Processes and Landforms*, *45*(9), 2063–2077. https://doi.org/10.1002/esp.4866

Magnin, F., Brenning, A., Bodin, X., Deline, P., & Ravanel, L. (2015). Statistical modelling of rock wall permafrost distribution: Application to the Mont Blanc massif. *Géomorphologie: Relief, Processus, Environnement*, *21*(2), 145–162. https://doi.org/10.4000/geomorphologie.10965

Matsuoka, N., & Murton, J. (2008). Frost weathering: Recent advances and future directions. *Permafrost and Periglacial Processes*, *19*(2), 195–210. https://doi.org/10.1002/ppp.620

Murton, J. B., Peterson, R., & Ozouf, J.-C. (2006). Bedrock fracture by ice segregation in cold regions. *Science*, *314*(5802), 1127–1129. https://doi.org/10.1126/science.1132127

Neely, A. B., DiBiase, R. A., Corbett, L. B., Bierman, P. R., & Caffee, M. W. (2019). Bedrock fracture density controls on hillslope erodibility in steep, rocky landscapes with patchy soil cover, southern California, USA. *Earth and Planetary Science Letters*, *522*, 186–197. https://doi.org/10.1016/j.epsl.2019.06.011

Paul, G. C. D. (1991). *Materials science & engineering*. CRC Press.

Pei, L., Blöcher, G., Milsch, H., Deon, F., Zimmermann, G., Rühaak, W., et al. (2016). Thermal strain in a water-saturated limestone under hydrostatic and deviatoric stress states. *Tectonophysics*, *688*, 49–64. https://doi.org/10.1016/j.tecto.2016.09.020

Phillips, M., Haberkorn, A., Draebing, D., Krautblatter, M., Rhyner, H., & Kenner, R. (2016). Seasonally intermittent water flow through deep fractures in an Alpine Rock Ridge: Gemsstock, central Swiss Alps. *Cold Regions Science and Technology*, *125*, 117–127. https://doi.org/10.1016/j.coldregions.2016.02.010

Prick, A. (1997). Critical degree of saturation as a threshold moisture level in frost weathering of limestones. *Permafrost and Periglacial Processes*, *8*(1), 91–99. https://doi.org/10.1002/(SICI)1099-1530(199701)8:1<91::AID-PPP238>3.0.CO;2-4

Rempel, A. W., Marshall, J. A., & Roering, J. J. (2016). Modeling relative frost weathering rates at geomorphic scales. *Earth and Planetary Science Letters*, *453*, 87–95. https://doi.org/10.1016/j.epsl.2016.08.019

Rode, M., Schnepfleitner, H., & Sass, O. (2016). Simulation of moisture content in alpine rockwalls during freeze–thaw events. *Earth Surface Processes and Landforms*, *41*(13), 1937–1950. https://doi.org/10.1002/esp.3961

Sass, O. (2005a). Rock moisture measurements: Techniques, results, and implications for weathering. *Earth Surface Processes and Landforms*, *30*(3), 359–374. https://doi.org/10.1002/esp.1214

Sass, O. (2005b). Spatial patterns of rockfall intensity in the northern Alps. *Zeitschrift für Geomorphologie: Supplementary Issues*, *138*, 51–65.

Segall, P. (1984). Rate-dependent extensional deformation resulting from crack growth in rock. *Journal of Geophysical Research*, *89*(B6), 4185–4195. https://doi.org/10.1029/JB089iB06p04185

Shmilovitz, Y., Enzel, Y., Morin, E., Armon, M., Matmon, A., Mushkin, A., et al. (2022). Aspect-dependent bedrock weathering, cliff retreat, and cliff morphology in a hyperarid environment. *GSA Bulletin*. https://doi.org/10.1130/B36442.1

Sibley, D. N., Llombart, P., Noya, E. G., Archer, A. J., & MacDowell, L. G. (2021). How ice grows from premelting films and water droplets. *Nature Communications*, *12*(1), 239. https://doi.org/10.1038/s41467-020-20318-6

Vlahou, I., & Worster, M. G. (2015). Freeze fracturing of elastic porous media: A mathematical model. *Proceedings of the Royal Society A: Mathematical, Physical & Engineering Sciences*, *471*(2175), 20140741. https://doi.org/10.1098/rspa.2014.0741

Walder, J., & Hallet, B. (1985). A theoretical-model of the fracture of rock during freezing. *Geological Society of America Bulletin*, *96*(3), 336–346. https://doi.org/10.1130/0016-7606(1985)96<336:ATMOTF>2.0.CO;2

Walder, J. S., & Hallet, B. (1986). The physical basis of frost weathering: Toward a more fundamental and unified perspective. *Arctic and Alpine Research*, *18*(1), 27–32. https://doi.org/10.2307/1551211

Zhang, Z. (2002). An empirical relation between mode I fracture toughness and the tensile strength of rock. *International Journal of Rock Mechanics and Mining Sciences*, *39*(3), 401–406. https://doi.org/10.1016/S1365-1609(02)00032-1